TRANSITION, DIFFRACTION AND SMITH-PURCELL DIAGNOSTICS FOR CHARGED PARTICLE BEAMS*

R. B. Fiorito†, Institute for Research in Electronics and Applied Physics, University of Maryland, College Park, MD 20742, U.S.A.

Abstract

I review the state of the art of diagnostics based on transition, diffraction and Smith Purcell radiation in the optical to millimeter wave band, which are currently being used to measure the transverse and longitudinal parameters of charged particle beams. The properties and diagnostic capabilities of the incoherent and coherent forms of these radiations are described. Examples of TR, DR and SPR diagnostics for electron and proton beams are presented.

INTRODUCTION

The spatial, angular and spectral distributions of radiation produced from a charged particle beam interacting with a material object or field, e.g. magnetic field, carries information about the beam properties. In this paper we review the state of the art in the diagnostic application of three important beam based radiations: transition, diffraction and spatially coherent diffraction from a grating, i.e. Smith Purcell radiation. These radiations, and indeed all radiation from charged particles, can be analysed using some fundamental concepts: 1) the radiation impact parameter; 2) the coherence length of radiation from a moving charge; 3) the resonance radiation condition for spatially coherent radiation from N_r radiators; and 4) the bunch coherence of radiation from N charges.

The radiation impact parameter $\alpha = \gamma\lambda/2\pi$ is the distance where the radial field of the charge is significant and therefore provides a convenient scale length for significant interaction of the charged particle's field with a medium. This property is analogous to the usually defined impact parameter which is the distance where a moving charged particle interacts with another charge.

For relativistic particles, the parameter α is also the effective source size of a virtual photon of wavelength λ, which is associated with the field of the moving charge. If the size of the radiator $r >> \alpha$, the radiator can be considered to be infinite and the radiation is transition radiation whose spectral angular density is frequency independent. If, however, $\alpha >\sim r$, or if the radiator is an aperture whose size $r <\sim \alpha$, the radiation produced is diffraction radiation (DR) and the spectral angular density is dependent on frequency and on the ratio r/α.

The radiation field of DR from a hole in an infinite radiator, TR from a complementary finite size solid radiator and TR from an infinite radiator are related by Babinet's principle[1] ,

$$E^{TR}_{\infty Screen} = E^{DR}_{Hole} + E^{TR}_{FiniteScreen}. \quad (1)$$

In this sense, TR from a finite screen can be considered to be a form of DR as Figure 1 suggests.

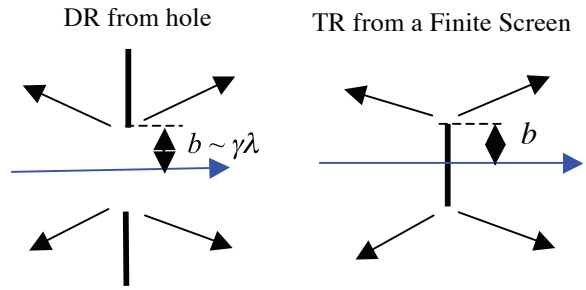

Figure 1. Diffraction and transition radiation from two complementary screens.

The coherence or "formation" length, as it is sometimes referred to in the literature, is the distance where the fields of the charge and the photon generated in the interaction defer in phase by π radians [2]. There are two types of coherence lengths, i.e. the vacuum coherence length, $L_v = (\lambda/\pi)(\gamma^{-2} + \theta^2)^{-1}$, which applies to the radiation produced when a charge moves from a medium into vacuum or vice versa; and the material coherence length, L_d which applies to a charge moving within a material with dielectric constant ε. Note that L_v is a function of the Lorentz factor γ for a relativistic charge while L_d is independent of γ. The definition of L_v indicates that for high energies and observation angle $\theta \sim 1/\gamma$, the coherence of TR or DR fields and the field a co-moving charge is maintained over distances in proportion to the square of the Lorentz factor. The phenomenon of interference of TR/DR from two foils or apertures in the path of a relativistic particle is an example where the vacuum coherence length plays a major role.

When the charge interacts with a series of radiators spaced periodically, e.g. a stack of foils or the periods of a grating, the radiation can be resonant, i.e. in phase, for a particular observation angle or wavelength [3]. Examples of resonance radiation are TR from a stack of foils and Smith Purcell radiation.

The last concept of interest to us is the coherence of charges in a bunch radiating in or out or phase. The general expression for the spectral angular density of any type of beam base radiation can be written in the form:

* Work supported by ONR and the DOD Joint Technology Office
† rfiorito@umd.edu

$$\frac{d^2I_N}{d\omega d\Omega} = \frac{d^2I_e}{d\omega d\Omega}\{N + N(N-1)S_\perp(k_\perp,\sigma_T)S_z(\sigma_z,k_z)\}, \quad (2)$$

where $S_{\perp,z} = |F(\rho_{\perp,z})|^2$ are, respectively, the transverse and longitudinal form factors, i.e. the squared moduli of the Fourier transforms of the corresponding charge densities and the first term on the RHS of Eq. (2) is the spectral-angular density of radiation produced by a single charge. When both of the form factors are of order unity, the radiation intensity is proportional to N^2 where N is the number of particles. This occurs at wavelengths close to or larger than the bunch length and the radiation is said to be fully *coherent*. At wavelengths much less than the bunch length the radiation is proportional only to N and the radiation is said to be *incoherent*. Both types of radiation serve useful purposes for charged particle beam diagnostics.

APPLICATIONS OF INCOHERENT RADIATION

Near Field Imaging using OTR and ODR

For most applications in rf accelerators the bunch micro pulse duration is of the order of 1 ps corresponding to a bunch length of about 300 microns. Hence the longitudinal form factor is small for observations of TR, DR and SPR at optical wavelengths and the radiation in this band is incoherent.

By far the most common use of incoherent OTR is beam imaging. For this purpose simply focusing a camera on the generating foil produces a linear, high resolution image of the beam. This application is commonly referred to as 'near field' imaging though the use of this term is not strictly accurate. For most situations OTR is the preferred beam imaging technique for monitoring the beam spatial profile. Figure 2 shows a comparison of OTR with other types of imaging screens,

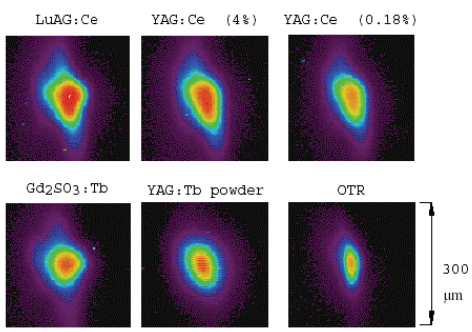

Figure 2: Comparison of e beam images using various screens at the 50 MeV BNL/ATF; from ref. [4]

i.e. phosphors and YAG crystals, which, although they produce a higher yield of photons, do not have the spatial and temporal resolution offered by OTR. OTR has been successfully used to image beams with micron spatial resolution (usually limited only by diffraction in the optics) and sub ps temporal resolution.

A number of theoretical studies [5-8] as well as experimental data have confirmed that the spatial resolution of OTR is primarily independent of energy and not related to the effective virtual photon source size $\gamma\lambda$ as some authors had previously claimed. An especially strong experimental confirmation of this fact is the successful OTR imaging of 100 micron size beams (confirmed by wire scanners) at a beam energy of 30 GeV, where $\gamma\lambda$ at optical wavelength is tens of millimeters [9].

OTR has been successfully used to image both relativistic electron and proton beams, e.g. the 120 MeV proton beam at FNAL [10], as well as non relativistic beams, e.g. the CLIC facility's 80 keV gun [11] and the University of Maryland's 10 keV electron beam ring (UMER)[12]. For the UMER source, OTR images have been taken in 10ns gates within a 100ns pulse showing the evolution of the beam profile[13].

Recently ODR near field imaging been demonstrated and used to determine horizontal beam position with respect to an edge radiator with an accuracy of 40 microns [14]. Experiment data comparing beam sizes using OTR as a baseline and ODR also indicated that ODR can provide relative beam sizes if the beam is Gaussian in x and y.

Figure 3. shows a comparison of an OTR image of a 7 GeV electron beam compared to the ODR image induced by the beam on a polished edge radiator that is 1.25mm away from the beam centroid as indicated by the dotted line. For 7 GeV the radiator impact parameter is about 1 mm at a wavelength of 500nm so that ODR is expected to be observed and the picture confirms this.

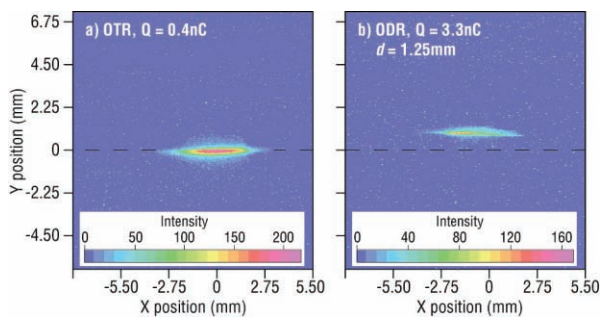

Figure 3: Near field mages of OTR (left) and ODR (right) from a 7 GeV beam passing through and near a polished metal edge, from ref. [14].

If the beam is moved in the horizontal direction, the centroid of ODR image tracks the motion as observed by beam position monitors in the walls of the accelerator tube. The results shown in Figure 4 indicated that the ODR centroid measurement linearly tracks the BPM signal to within 40 microns. The ultimate accuracy of this

ODR beam position monitor is expected to be 10 microns or less.

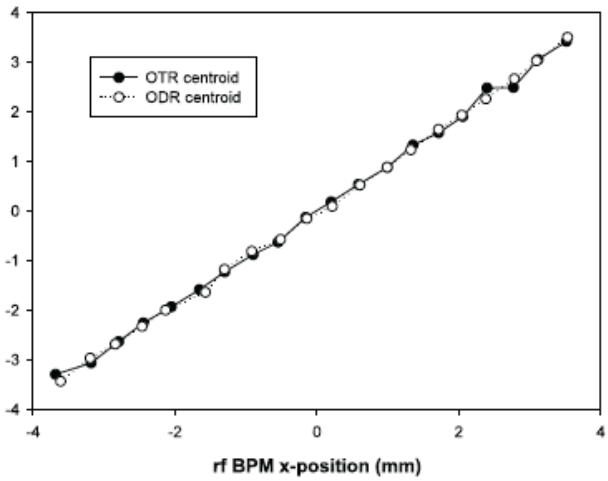

Figure 4: Centroid of ODR and OTR images vs. horizontal BMP signals illustrating the tracking of ODR with horizontal beam position; from ref. [14]

Far Field Imaging of OTR and ODR

The far field images of OTR from a single foil, and interference of OTR two foils and ODR-OTR produced when the first foil is a metal micromesh, have all been demonstrated to be useful as beam divergence and energy diagnostics for relativistic electron beams.

In order to use such far field images to measure divergence, a model for the distribution of trajectory angles is assumed, e.g. a single Gaussian distribution function, f(x',y'). This expression is then convolved with the angular distribution for a single electron. Horizontal (x') or vertical (y') line scans of the resulting angular distribution are then fit to the experimental data to provide the divergences.

Figure 5 shows *single foil* OTR angular distributions for three different beam conditions at the 48 MeV CLIC test facility, along with corresponding intensity line scans. Fits of these scans produce divergences show on the line scan graph. Using the angular distribution of OTR from a single foil, divergences as low as 0.1/γ can be measured.

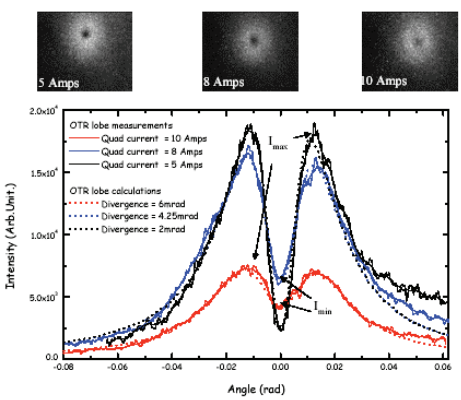

Figure 5: Far field single foil OTR patterns for three different divergences (top); line scans (bottom); from [15]

Figure 6 shows an two foil OTR interferogram which was taken to measure the divergence of the NPS 100 MeV linac, which has an average current of about 0.1 μA. The picture was taken with a high quantum efficiency cooled CCD camera and an optical interference filter with sufficiently narrow band pass to insure that the visibility of the fringes is dominated by beam divergence.

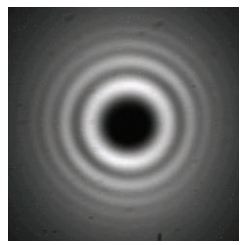

Figure 6: OTRI from a 100 MeV electron beam.

Divergences as low as 0.01/γ have been measured with two foil OTRI and ODTRI [16]. Simultaneously, the energy of the beam can be determined from the interference peaks with accuracy of about 1% and under the right conditions, energy spread can also be determined [17].

If the beam is magnetically focused to an x or y waist condition at the second foil of the interferometer, and simultaneous imaging of the spatial and angular distributions is performed, a corresponding x or y *rms* emittance measurement can be made [18]. This can be accomplished with a variable focus lens, or two cameras one focused on the foil, the other to infinity.

An extension of this technique called optical phase space mapping can also be done with the help of a movable optical mask. In this method the beam is first imaged onto a pinhole mask. The far field AD pattern emerging from the pinhole is then analysed with the same technique described above to provide a localized (i.e. within the beam distribution) measurement of the divergence and ensemble trajectory angle. By scanning the pinhole over the beam image, which is monitored by another camera focused on the back of the mask, a map of the (x,x') or (y,y') trace space of the beam can be constructed [19].

The angular distribution of ODR from a single edge, slit or any type of symmetric aperture can also be used as a diagnostic. However, unlike OTR, the AD of ODR depends not only on the divergence but the beam size and offset from the center of the aperture used to create the radiation. Hence the analysis of the AD of ODR a diagnostic for a particular parameter is more complex than OTR. Nevertheless, a number of methods employing the near field and far field distributions of ODR have been suggested [20,21].

For beams with very low divergence, the AD of ODR is mainly dependent on the beam size or position within the aperture [21]. For an aperture with vertical or horizontal symmetry e.g. a slit, the position effect can be neutralized by positioning the beam in the center of the aperture. In

cases where the effect of divergence cannot be neglected two orthogonal slits can be used to separately measure the (x,y) sizes and the (x',y') divergences [22]. Efforts to provide beam size diagnostics using the far field ODR AD are underway by a number of groups [23,24].

Measured and fitted scans of a far field ODR angular distribution pattern from a 700 MeV passing through the center of a 0.5 mm slit is shown in Figure 7 which is taken from [24]. The beam size and divergence from

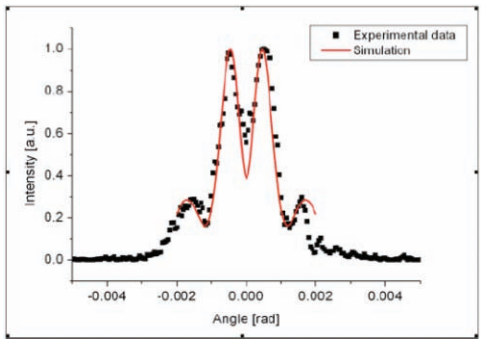

Figure 7. Measured and fitted vertical scans of AD image of ODR with a 800nm band pass filter

the fit are: 70μ and 30μrad respectively. A significant problem in obtaining useful far field ODR data is the interference of optical synchrotron radiation produced by from upstream magnets with ODR from the slit.

Far field ODR can also be used in conjunction with OTR as in an ODR-OTR interferometer to measure divergence [16]. In this configuration a micromesh foil with hole dimensions d ≤10μ << R, the beam size. The ODR is produced both from the wires and holes of the mesh interfere with OTR from a mirror and create interferences. The wire thickness and density is chosen so that the fringes created by ODR and OTR from electrons intersecting the wires are heavily scattered so that their visibility is zero. The ODR-OTR fringes from the unscattered particles passing through the mesh holes then seen above a smooth background; the visibility of these fringes provides a divergence diagnostic. Note that the divergences measured with this technique is not limited to beam divergences which exceed the mean scattering angle in the first foil, as is the case with a conventional OTR interferometer.

Figure 8 shows scans from an ODTR and an OTR interferograms for the same beam conditions and the same measured divergence. The foil thickness and material of the first foil of the OTR interferometer was chosen to introduce negligible scattering to validate the ODTRI divergence measurements.

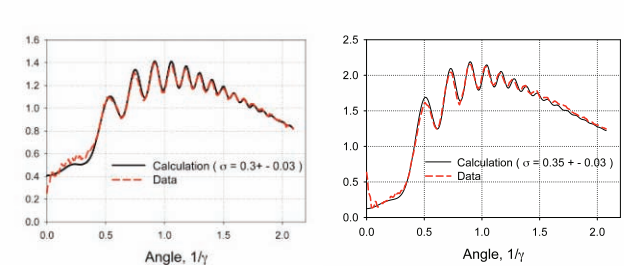

Figure 8: Comparison of divergence measurements with an ODTR (left) and OTR (right) interferometers [16].

COHERENT RADIATION BUNCH LENGTH DIAGNOSTICS

The use of fully coherent radiation such as transition, diffraction and Smith Purcell radiation have been used to diagnose transverse as well as longitudinal properties of beams. We will confine our discussion to longitudinal beam diagnostics making use of the dependence of the coherent radiation on the longitudinal form factor of the beam, cf. Eq. (2). The chief advantages of frequency based diagnostics are their bandwidth which easily exceeds the equivalent temporal limit imposed by conventional streak cameras (currently about 0.3 ps) and lower cost.

The most common types of spectral measurements are: 1) direct spectroscopy, which employ dispersive gratings and/or multiple detectors; 2) autocorrelation techniques which use scanning or single shot interferometers; and 3) electro-optic sampling techniques. Items 1) and 2) have been well described in the literature and item 3) is reviewed in the invited talk by van Tilborg presented in these Proceedings [25].

We will therefore discuss only two recently developed techniques which both employ the frequency dependence of the *angular distributions* of coherent TR, DR and Smith Purcell radiation (SPR) to measure bunch length.

CDR and CTR Angular Distribution Method

We have noted above that the angular distributions of TR from a finite sized foil and DR from an aperture are both forms of diffraction radiation and hence the single electron spectral angular densities of both radiations are frequency dependent, i.e. the first term on the RHS of Eq. (2). This frequency dependence adds an additional complication to the analysis of the spectrum of coherent radiation, since it is the goal of spectral analysis to measure the form factors in order to determine the bunch size.

It is possible to use and optimize the sensitivity of the AD of CTR and CDR for a given bunch length and beam energy to frequency in the band required to adequately sample the form factor. To do this we control the size of the radiator r, so that the radiation impact parameter $\alpha \sim \gamma c \Delta t_b / 2\pi \sim r$ where Δt_b is the expected bunch length and $1/\Delta t_b$ is the frequency band of interest. For a 10 MeV and a 1 ps bunch width, e.g. the optimum radiator size is about 8mm.

The broad band AD is calculable from theory by taking the radiated power of CTR or CDR for a given radiator and geometry per electron from theory, assuming a model for the bunch distribution, e.g a Gaussian, calculating the resultant form factors, multiplying by the form factor for a particular bunch length and integrating over the

appropriate frequency range. The mathematical details are presented in [26,27], so we will only present results for the example mentioned above.

The frequency band necessary for the calculations is determined by both the high frequency role off of the bunch form factor and the low frequency role off due to the finite size of the radiator. These are illustrated in Figure 8 for three Gaussian longitudinal distributions.

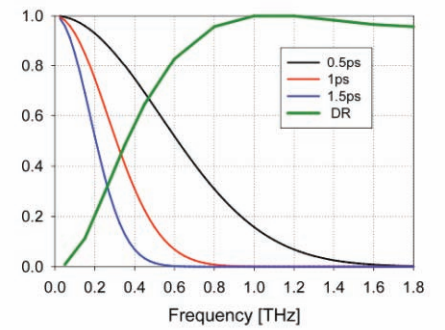

Figure 9: Gaussian bunch form factors in black, red and blue for bunch lengths 0.5, 1.0 and 1.5ps respectively; green: DR spectrum for an 8mm diameter disk.

To illustrate the effect of bunch length on the AD of DR from a finite radiator, we calculate line scans of the projected AD on a plane 300mm away from the source. Sample frequency dependent scans within this range of frequencies are shown in Figure 10, and total (frequency integrated) angular distributions scans for three different bunch lengths are presented in Figure 11.

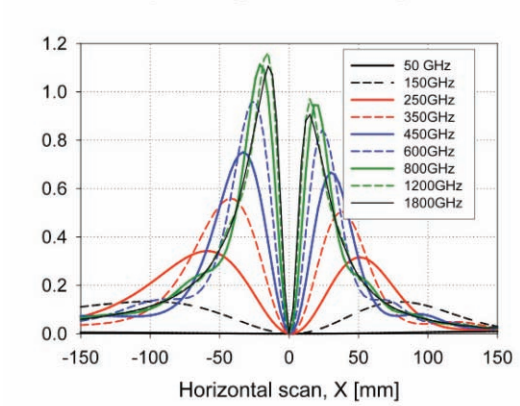

Figure 10: Horizontal line scans of the angular distribution of CDR from an 8mm disk projected onto a plane at 300mm from the source for various frequencies in the band 50-1800 GHz.

A proof of principle experiment using the AD of CTR from a finite rectangular plate and CDR from a slit has recently been performed at the Paul Scherrer Institut's SLS 100 MeV linac [26]. Two different bunch compressor settings produced bunch lengths: 0.7 and 1.0 ps, which have been previously measured at PSI using an electro-optic sampling method. Simple vertical and horizontal line scans through the AD's of the CTR and

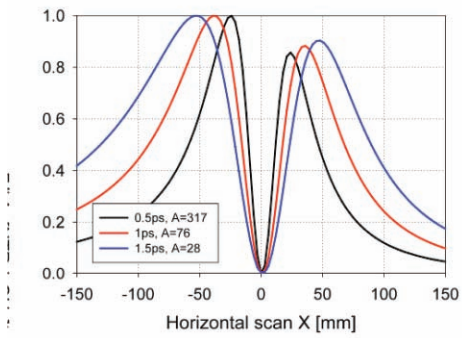

Figure 11: Broad band (frequency integrated) scans of the projected AD's of CDR at 300mm from the source; A is the amplitude scale factor for each curve.

CDR were measured by a Golay cell placed on an x, y translation stage. The frequency response of the cell is nearly flat over the frequency range 50-2000 GHz.

Figure 12 shows the results of fitting the AD of DR from a 10 mm slit in a 40x40mm plate produced using the procedure mentioned above assuming a Gaussian beam pulse with a 0.78 ps full width at half maximum with data obtained by vertical line scan of the measured AD. Data from a solid 40x40mm rectangular plate, used to generate CTR, was also fit with the same bunch width used for the fit of the slit CDR scan data shown in Figure 12. The Figure shows the overall *rms* deviation of the fit. PBU0 identifies the bunch compressor setting used to produce a sub ps bunch. The bunch lengths measured with the slit

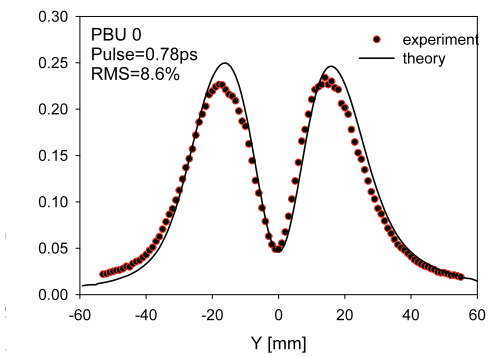

Figure 12: Vertical line scan of AD of CDR from a slit at 300mm from the source; from [26].

and the solid rectangular targets agree with each other, within experimental uncertainty, as well as with previous EO measurements, indicating the consistency and validity of the method.

Coherent Smith Purcell Bunch Length Monitor

The final diagnostic method to be reviewed in this paper is the coherent Smith Purcell effect. The SP effect is observed when an electron beam passes over a grating [28]. A spectrum of light is observed emanating from the grating as shown in Figure 13. The condition for generation of SP radiation follows the relation:

$$\lambda = \frac{l}{n}(\beta - \cos\theta) \qquad (3)$$

where λ is the observed wavelength, l is the number of grating periods, n is the order of the radiation, and θ is the angle of observation. One can conclude from our earlier discussion of DR and the condition for resonance radiation that the SP effect is actually resonant DR from a series of edges and it has been analyzed as such [29].

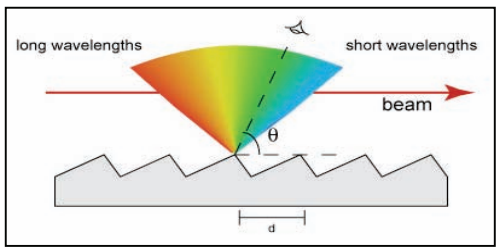

Figure 13: Illustration of the Smith Purcell effect.

Thus it is clear that 1) substantial generation of incoherent SP radiation will occur when the distance between the beam and the grating is close to the radiation impact parameter α; 2) a fully coherent form of the radiation (CSPR) is possible when the emitted wavelengths are comparable to or longer than the bunch size; 3) like DR from any radiator, the wavelength and bandwidth of CSPR depends on the properties of the radiator itself, in this case the grating period and the geometry of one period of the grating; and 4) that the band width can be optimized for a given beam energy to measure the bunch form factor for the expected bunch size.

Several international efforts are presently studying CSPR as a bunch length diagnostic. These cover a range of electron beam energies from 6 MeV to 30 GeV [29-33]. However, I will confine my discussion to what in my assessment is the most developed of these, i.e. the work by the MIT-Bates group [32,33].

The intensity of SPR for a single electron has been derived [34]. If this relation is put into Eq. (2) and integrated over the transverse form factor of the bunch one obtains an expression for the frequency dependent spectral density of the radiation [32]. The resonance condition given by Eq. (3) links the wavelength or frequency of SPR with the angle of observation. Thus a scan of the angular distribution of CSPR is linked to the spectral distribution.

If one models the longitudinal distribution, e.g. by a single Gaussian, multiplies the spectral density of the SPR by the corresponding form factor (also a Gaussian) and fits this to measured angular-spectral distribution, one can measure the bunch length in a manner similar to what is described above. Unlike in the case of normal DR from a single aperture or medium, it is not necessary to integrate the SPR over the bandwidth since the angle and frequency are correlated via Eq. (3).

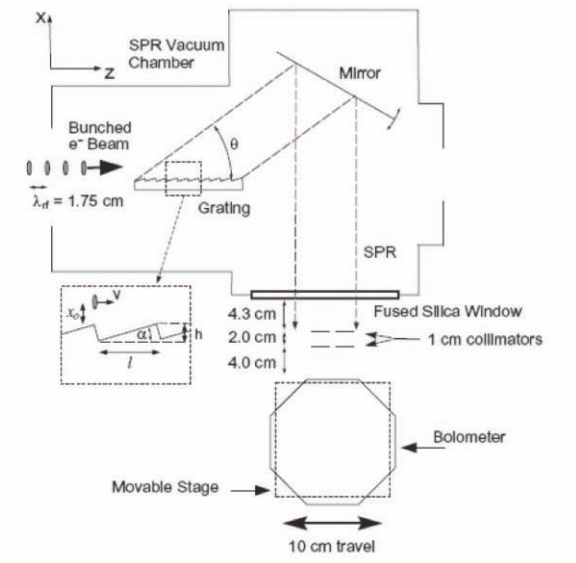

Figure 14: Schematic of the MIT experimental setup to measure the angular/spectral distribution of CSPR.

Experiments at 15 MeV for various bunch lengths in the range of 0.5 to 1ps have been performed at the MIT Bates accelerator laboratory where mm wavelength CSPR has been observed. The experimental setup is shown in Figure 14 which is taken from ref. [32]. A scanning bolometer is used to observe the angular distribution of the radiation in a manner similar to the CDR experiments described above.

Figure 15 also from [32] shows the measured and fitted angular distribution of CSPR assuming a single Gaussian bunch shape with a bunch length of 0.6±0.2 ps. This value has been confirmed by independent measurements.

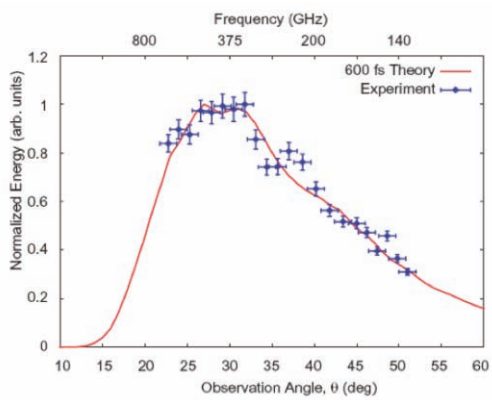

Figure 15: Data and fit of the angular distribution of CSPR for a Gaussian longitudinal distribution with a FWHM of 600 fs.

CONCLUSIONS

We have briefly reviewed the state of the art in TR, DR and SPR diagnostics for charged particle beams. Diagnostic applications of these beam based radiations continue to advance and become more refined. DR and SPR diagnostics hold particular interest since they are non -interceptive in nature and therefore are potentially applicable to diagnose very high current density beams. ODR diagnostics in particular have the potential to measure multiple beam parameters by observation of the near and far field distributions of the radiation.

Both the incoherent and coherent forms of these radiations can be utilized to measure the transverse and longitudinal properties of the beam. Examples of several diagnostic applications of the spatial and angular distribution of incoherent OTR and ODR for imaging the beam and measuring its divergence and energy have been presented. Additionally two methods employing the angular distributions of CDR and CSPR to measure bunch length in the FIR-mm band have been reviewed here. The observation of coherent transition radiation at shorter wavelengths, i.e. in the optical band, have been reported in the literature and in one case the effect of the *transverse* form factor on the far field angular distribution of COTR interferences has produced a novel beam size diagnostic [35]. Coherent optical TR, DR and SPR also have the potential to serve as diagnostics for micro bunching at optical wavelengths, which has recently been observed e.g. at LCLS [36].

REFERENCES

[1] A. G. Shkvarunets, R.B. Fiorito and P.G. O'Shea, Nuc. Instrum. and Methods B., 201 (1), pp. 153-160 (2003).

[2] L. Wartski, et. al., J. Appld. Phys., 46, 3644 (1975).

[3] M. Ter-Mikaelian, High Energy Electromagnetic Processes in Condensed Media, Wiley-Interscience, (1972).

[4] A. Murokh, et. al., Proceedings of 2001 Particle Accelerator Conference, IEEE, pp. 1333-35, (2001).

[5] D.W. Rule and R.B. Fiorito, AIP Conf. Proc. No. 229, p. 315,(1991).

[6] X. Artru, et. al. Laboratoire de l'Accelerateur Lineaire Report No. 97-30, (1997).

[7] M. Castellano and V. Verzilov, Phys. Rev. ST Accel. Beams 1, 062801 (1998).

[8] V. A. Lebedev, Nucl. Instrum. Methods Phys. Res., Sect. A, 372, p. 344 (1996).

[9] P. Catravas, et. al., IEEE, Proc. of PAC99, vol. 3, p. 2111-2113 (1999).

[10] V. Scarpine, et. al. , Proc. of PAC07, p. 2639, (2007).

[11] C. Bal, et. al., Proc. of DIPAC03, p. 95, (2003).

[12] R. Fiorito, et.al., Proc. of PAC07, p. 4006, (2007).

[13] K. Tian, et. al., Phys. of Plasmas, 15, 056707 (2008).

[14] A. Lumpkin, et. al., Phys. Rev. ST Accel. Beams 10, 022802 (2007).

[15] E. Bravin and T. Lefevre, Proc. of DIPAC03, p. 92, (2003).

[16] R. Fiorito, A. Shkvarunets, T. Watanabe, V.Yakimenko and D. Snyder, Phys. Rev. ST Accel. and Beams, 9, 052802 (2006).

[17] R. B. Fiorito and A.G. Shkvarunets, Proc. of DIPAC03, Mainz, DE, p.89 (2003).

[18] R.B. Fiorito and D.W. Rule, AIP Conf. Proc. 319, p.21-37, ed. R. Shafer (1994).

[19] R. Fiorito, A. Shkvarunets and P. O'Shea, AIP Conf. Proc. 648, p. 187-194, ed. G.A. Smith and T. Russo, AIP (2002).

[20] M. Castellano, Nucl. Instrum. Methods Phys. Res., Sect. A , 394, 275 (1997).

[21] R.B. Fiorito, D.W. Rule and W. Kimura, AIP Conf. Proc. 390, ed. A. Lumpkin, pp. 510-517, (l997).

[22] R.B. Fiorito and D.W. Rule, Nuc. Instrum. and Methods B, 173, 67-82 (2001).

[23] P. Karataev, et. al,, Phys. Rev. Lett. 93, 244802 (2004).

[24] E. Chiadrioni, et. al., paper FRPMN027. Proc. of PAC07, Albuquerque, New Mexico, USA (2007)

[25] J. van Tilborg, "Electroptic Techniques in Beam Diagnostics,",Paper TUIOTIO01, Proc. of BIW08.

[26] A.G. Shkvarunets, R.B. Fiorito, V. Schlott and F. Mueller, Paper WEPC21, Proc. of DIPAC 07

[27] A.G. Shkvarunets and R.B.Fiorito, Phys. Rev ST Accel. and Beams, 11, 012801 (2008).

[28] S. Smith and E. Purcell, Phys. Rev. 92, 1069 (1953).

[29] A. Potylitsin, Nuc. Instrum. and Methods B, 145, Number 1, 2, pp. 60-66(7) (1998).

[30] G. Doucas, et. Al. Phys. Rev. ST Accel. Beams 5, 072802 (2002).

[31] G. Kube,et al., Phys. Rev. E 65, 056501 (2002)

[32 S. Korbly, et. al. Phys. Rev. ST Accel. Beams 9, 022802 (2006).

[33] S. Korbly, et. al. Phys. Rev. Lett. 94, 054803 (2005).

[34] P.M. van den Berg, J. Opt. Soc. Am. 63, 1588 (1973).

[35] A. Lumpkin, et. al., Proceedings of the 2004 FEL Conference, p. 519-522, Trieste, Italy (2004).

[36] D. Dowell, et. al.,Proc. of the 2007 FEL Conference, p. 276, Novosibirsk, Russia (2007).